PWM as a Low Cost Method for the Analog Control of MEMS Devices

Corey Pollock, Lawrence K. Barrett, Pablo G. del Corro, Alexander Stange, Thomas G. Bifano, and David J. Bishop

***Abstract*— In this paper, we discuss the use of pulse width modulation (PWM) to control analog MEMS devices. We achieve a precise linear analog control of MEMS by applying PWM signal with a frequency well above the system's mechanical natural frequency. We first demonstrate this using a parallel plate actuator and comb-drive, and then extend the technique to control a commercial deformable mirror. Such an approach allows the system designer to replace expensive drive electronics such as the high precision DACs and high voltage, linear amplifiers with a simple on-off switch. The advancements in the electronics industry tend to make precise timing cheaper and faster; our approach exploits these long-term trends to create low-cost control circuits. We also show how PWM control can linearize the positional response of the devices, where typically the position would depend quadratically on the applied analog voltage.**

***Index Terms*— Microelectromechanical systems, pulse width modulation, electrostatic actuator, linearize.**

I. Introduction

MICROELECTROMECHANICAL systems (MEMS) have become a technological solution of choice for many advanced applications and currently are a roughly $20B/year industry. They are small, fast, and robust with a wide range of sensing and actuating capabilities. Using semiconductor manufacturing methods, they can be quite inexpensive to build. One broad class of MEMS use actuators to achieve mechanical motion in response to applied electrical inputs. Examples include micromirrors [1]–[3], shutters [4], valves [5], RF filters [6], [7], nanopositioners [8]–[11] and atomic writing systems [12]. MEMS actuators can be built using a wide range of driving methods including electrostatic [13]–[16], electromagnetic [17], [18], thermal [19]–[21] and piezoelectric [22] techniques. Some actuators are digital, the presence or absence of a signal turns something on or off, but most require analog control. A deformable mirror (DM) is an example requiring analog control where the surface shape of a deformable membrane is distorted by a spatially distributed array of actuators to change the wavefront of reflected light.

In electrostatic and piezoelectric devices, the control signal is usually a high voltage, low current signal, typically in the 50-250 volt range. Thermal devices normally use a few volts of drive at a few tens of milliamps of current and electromagnetic drives might require a volt or two at hundreds of millamps. The electronic circuits for controlling MEMS devices have special requirements, well beyond typical analog circuits, and can be expensive. For many electrostatic systems, there is a digital control system (usually a microprocessor), a high precision Digital to Analog converter (DAC) and a linear, high voltage (HV) amplifier. These drive circuits need high precision and modest speeds. It is not uncommon in a commercial device for the drive electronics to be far more expensive than the MEMS chip itself, severely restricting MEMS as a low cost solution.

Pulse width modulation (PWM) is a drive technique that uses pulses of varying widths to achieve analog control. It is commonly used to control the speed of DC motors but it has also been used to control MEMS such as the dimming in a optical system [23], [24], the flow through a microfluidic valve [5], [25], and to control thermal actuators [26]. Such a drive scheme has a number of advantages over conventional approaches. In an electrostatic system, one can replace the precision DAC and linear HV amplifier with a simple on-off switch. Timing is digital and cheap, whereas analog control is not. The electronics industry continues to research and develop faster transistors [27]–[30], and PWM control can leverage these gains. Given that most systems are controlled with a microprocessor, the timing essentially comes for free and integrating a DC power supply and HV switch completes the control circuit. As an example, with a 1 kHz MEMS device and a 1 GHz processor, one can use a 10 kHz PWM drive with nanosecond timing control to provide the equivalent of a 17 bit DAC. Another advantage, as we show below, is that PWM linearizes the response of the system. Typically, the position of an electrostatic device depends quadratically on applied voltage whereas for PWM control, the position is a quasi linear function of duty cycle.

Manuscript received August 24, 2018; revised November 2, 2018; accepted December 23, 2018. Date of publication January 14, 2019; date of current version April 2, 2019. This work was supported in part by the Engineering Research Centers Program of the National Science Foundation under NSF Cooperative Agreement EEC-0812056, in part by the DARPA Atoms to Products (A2P) Program/Air Force Research Laboratory (AFRL) under Contract FA8650-15-C-7545, in part by the National Science Foundation under NSF Cooperative Agreement ECCS-1708283, and in part by the Engineering Research Centers Program of the National Science Foundation under NSF Cooperative Agreement EEC-1647837. Subject Editor A. Zhang. *(Corresponding author: Corey Pollock.)*

C. Pollock and T. G. Bifano are with the Mechanical Engineering Department, Boston University, Boston, MA 02215 USA (e-mail: cpollock@bu.edu).

L. K. Barrett and A. Stange are with the Materials Science and Engineering Division, Boston University, Boston, MA 02215 USA.

P. G. del Corro is with the Laboratoire de l'Intégration du Matériau au Systéme, Université de Bordeaux, 33600 Pessac, France.

D. J. Bishop is with the Materials Science and Engineering Division, Mechanical Engineering Department, Department of Electrical and Computer Engineering, Department of Physics, Department of Biomedical Engineering, Boston University, Boston, MA 02215 USA.

Digital Object Identifier 10.1109/JMEMS.2019.2891205

1057-7157 © 2019 IEEE. Translations and content mining are permitted for academic research only. Personal use is also permitted, but republication/redistribution requires IEEE permission. See http://www.ieee.org/publications_standards/publications/rights/index.html for more information.

This paper investigates the use of PWM to control three different analog electrostatic MEMS systems, (1) a single parallel plate mass sensor, (2) a comb-drive actuator used for writing with atomic beams, and (3) a commerical DM that can be reshaped dynamically using an array of parallel plate actuators. Although similar PWM methods have been used [31]–[34], this work focuses on the analog control and the cost savings of this technique. We first present the theoretical derivation of PWM control and the linearization of the electrostatic devices. Then we analyze and discuss the results from the three systems. While this paper focuses on electrostatic drives, the PWM approach is general and works equally well with any type of drive (e.g. thermal, piezoelectric, magnetic).

II. Theory

This work investigates two types of electrostatic actuators, (1) a parallel plate capacitor and (2) a comb-drive. This section describes the theory of using PWM to drive these actuators. A graphic model for each system is shown in Fig. 1, both of which can be approximated as linear systems described by the differential equation:

$$m\ddot{x} + b\dot{x} + kx = F(t), \tag{1}$$

where m is mass, b is the damping coefficient, k is the spring constant, x is position, $\dot{x}$ is velocity, $\ddot{x}$ is acceleration, and $F(t)$ is an externally applied force. Throughout this work we drive the MEMS with a PWM signal (i.e. pulse wave, rectangular wave) switching between zero force and a maximum force, F_0, at a frequency, ω. We demonstrate in this section that if ω is much greater than the system's natural frequency, the effective force on the mass becomes $F_0 R_{DC}$, where R_{DC} is the duty cycle (value 0-1). The Fourier series of the forcing function described above is:

$$F(t) = F_0 R_{DC} + F_0 \sum_{n=1}^{\infty} \frac{2}{n\pi} sin(n\pi R_{DC}) cos(n\omega t), \tag{2}$$

where $F(t)$ is the force, t is time (seconds) and ω is frequency (rad/s). This can be separated into two forces, F_1 and F_2, defined as:

$$F_1 = F_0 R_{DC}, \tag{3}$$

$$F_2 = F_0 \sum_{n=1}^{\infty} \frac{2}{n\pi} sin(n\pi R_{DC}) cos(n\omega t). \tag{4}$$

The response of a linear system may be represented as the superposition of responses from multiple force inputs. This is described mathematically as $x(t) = x_1 + x_2$, where x_1 and x_2 are the position responses of F_1 and F_2 respectively. We first investigate x_2. F_2 is the summation of sinusoidal forces and one method of solving the steady state solution of a sinusoidal input is to use the transfer function of the system, with the solution being equal to the sinusoidal input times the transfer function. The transfer function of a mass spring system is [35]:

$$\frac{x}{F(t)} = \frac{1}{m\sqrt{(\omega_n^2 - (\omega)^2)^2 + (2\zeta\omega_n\omega)^2}}, \tag{5}$$

where $\omega_n = \sqrt{\frac{k}{m}}$ is the natural frequency of the system and $\zeta = \frac{2\omega_n}{b}$. We can then multiply the transfer function by each summation term in (4). When making this step, we must also substitute ω with $n\omega$, since $n\omega$ is the frequency in each summation term. Therefore the position response of F_2 is:

$$x_2 = F_0 \sum_{n=1}^{\infty} \frac{2}{n\pi} \frac{sin(n\pi R_{DC}) cos(n\omega t)}{m\sqrt{(\omega_n^2 - (n\omega)^2)^2 + (2\zeta\omega_n n\omega)^2}}. \tag{6}$$

Next we look at the response from F_1, which we can plug directly into (1). Since we are solving for the steady state solution $\ddot{x} = \dot{x} = 0$ and we are left with only the opposing spring force. This results in:

$$x_1 = \frac{F_0 R_{DC}}{k}. \tag{7}$$

From (6) we see that if $\omega >> \omega_n$, the sinusoidal response, x_2, approaches zero. This agrees with the known frequency response of a harmonic oscillator. As the driving frequency increases beyond the natural frequency, the amplitude of the response decreases by 40 dB/decade. This means that if we drive a mass with a PWM signal at a frequency much greater than the natural frequency, x_2 goes to zero and we are left with (7) defining our steady state solution. This solution is true for all linear mass spring damper systems driven by a PWM signal.

Conceptually, imagine hitting a child's swing with baseballs. If the frequency of baseballs hitting the swing is comparable to or below the swing's natural frequency, the swing will move appreciably between impacts of the ball. However, if the balls hit the swing at a rate far in excess of the swing's natural frequency, the swing stays in a static position. The relaxation of the swing's position is negligible in comparison with its static displacement. By changing the specific impulse transferred to the swing, its position can be continuously controlled in exactly the same way one would control its position by adjusting an analog force.

Next, we look at the specific cases of the electrostatic actuators where we substitute F_0 with the electrostatic force, F_e. In this case, we use a PWM signal for the voltage which then produces a PWM signal for the electrostatic force. One of the assumptions in the above equations is that the force is switching instantaneously. To extend these results to the electrostatic force, the electrical response time of these actuators must be much faster than the period of the PWM signal. The fastest frequency we use is 2 MHz. The parallel plate capacitors and comb-drives we test have an electrical time constant, (τ), less than a nanosecond. This is much faster than the period of our signal and therefore we can assume the electrostatic force matches the PWM signal.

The first actuator we will look at is a parallel plate capacitor. In general, the electrostatic force across a capacitor is:

$$F_e = \frac{1}{2}\frac{dC}{dx}V^2, \tag{8}$$

Using a parallel plates model, the electrostatic force between two plates is [36]:

$$F_e = \frac{\epsilon A V^2}{2(g_0 - x)^2}, \tag{9}$$

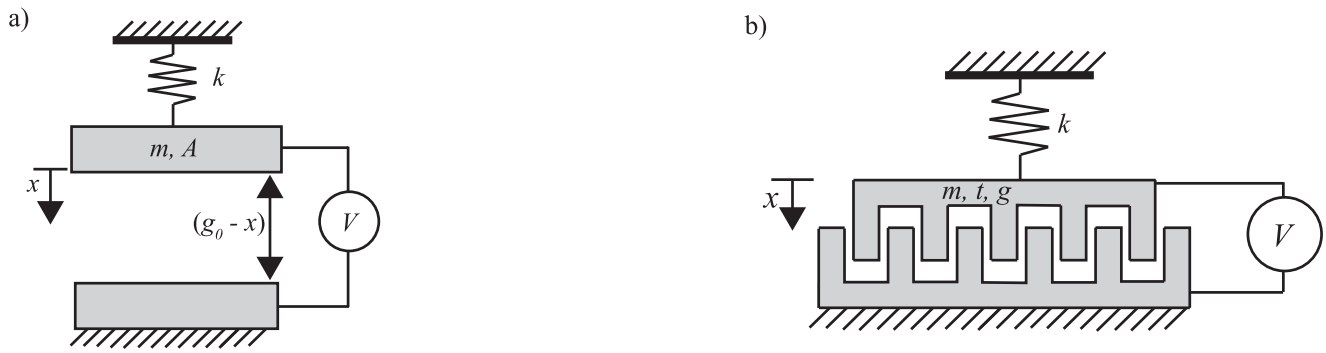

Fig. 1. **Electrostatic Actuator Models:** a) Parallel plate capacitor where A is the plate area and g_0 is the gap between the plates. b) Comb-drive actuator where t is the comb thickness (out of plane) and g is the lateral gap (perpendicular to x) between comb fingers. In both figures m is the mass of the movable plate or combs, k is the spring constant, x is the displacement, and V is the applied voltage difference.

where ϵ is the medium's permittivity, A is the area of the plate, V is the PWM voltage, g_0 is the pre-actuation gap between the stationary and moving plates and x is the displacement of the moving plate. When controlling the displacement of the plate with voltage control, the plate initially has a quadratic response with respect to voltage for small values of x. However, as x approaches 1/3 of g_0 (pull-in position [37]), the response deviates from a quadratic curve and $\frac{dx}{dV}$ approaches infinity, resulting in an unstable system. When this same system is driven with a PWM signal, the resulting force on the mass is $F_e R_{DC}$, with V^2 constant. With this change, the response is now linear with respect to the duty cycle for small values of x. With a constant force, the position would be truly linear with respect to the duty cycle, however in the case of the parallel plate capacitor, the force, F_e, changes with displacement. As x approaches the pull-in position, the response becomes nonlinear and eventually becomes unstable, similar to the response of a conventional analog control.

We now turn our attention to a comb-drive. If we again assume a parallel plate model, the electrostatic force is [36]:

$$F_e = \frac{\epsilon n t V^2}{g}, \tag{10}$$

where n is the number of interdigitated fingers, t is the comb thickness, and g is the gap between the fingers. One of the glaring differences between the comb-drive and parallel plate is that there is no x term in the comb-drive force. This means the force does not depend on the displacement and with a constant voltage, V, F_e is constant. This leads to a linear solution to (7) with respect to the duty cycle. By simply changing the method of control from voltage to PWM, we effectively linearize the system. It is worth noting that (10) is subject to error because fringe field effects contribute significantly to the capacitance of the device. Although the predicted force and capacitance are low, we show in the subsequent section that the predicted linear relationship is still accurate.

In general, PWM can be used in conjunction with a low pass filter to provide smooth precise analog control of a MEMS system. One method is to use the force generating system as a filter. This is how many thermal MEMS are driven with PWM [26]. In this scenario the thermal system is slower than the PWM frequency and acts as a low pass filter, resulting in an analog temperature and therefore an analog mechanical response. The method discussed in this paper and described mathematically above uses a force (electric field) that responds faster than the PWM frequency but is applied to a slower mechanical system. This results in the mechanical system acting as the low pass filter. For this last scenario the system must meet two requirements: (1) the force (e.g. electric field, magnetic field, temperature) must have a response time much faster than the PWM driving frequency and (2) the driving frequency must be much faster than the mechanical natural frequency.

TABLE I
STEADY STATE TESTING SUMMARY

	Parallel Plate	Comb-drive	DM
Natural Freq.	20 kHz	1 kHz	100 kHz
PWM Freq.	300 kHz	50 kHz	700 kHz
PWM Voltage	2 - 3.5 V	20 - 50 V	92 V
***Amp. Tech.**	None	Trek2100	Switching Circuit
Meas. Tech.	Zygo	SEM	Zygo

*Each device uses a function generator to generate the PWM signal.

III. Results and Discussion

In this section we describe each of the three MEMS devices in detail and discuss their experimental results. The first is a parallel plate capacitor, an electrostatic, out of plane, trampoline-type device. The second is a comb-drive linear in-plane actuator. These two fit the models presented in Fig. 1 well and provide a test bed for the theory discussed above. The final device is a commercial MEMS device, a DM manufactured by Boston Micromachines Corporation. Due to the geometry of the DM, it does not match the linear model as well, however we show that it can still be effectively driven with PWM. Each device has different setup requirements and we cover each in detail in the subsequent sections. The setups are also summarized in Table I.

A. Parallel Plate Actuator

Fig. 2a shows a scanning electron microscope (SEM) image of the parallel plate actuator. It was made using the PolyMUMPs process from MEMSCAP. The actuator consists of

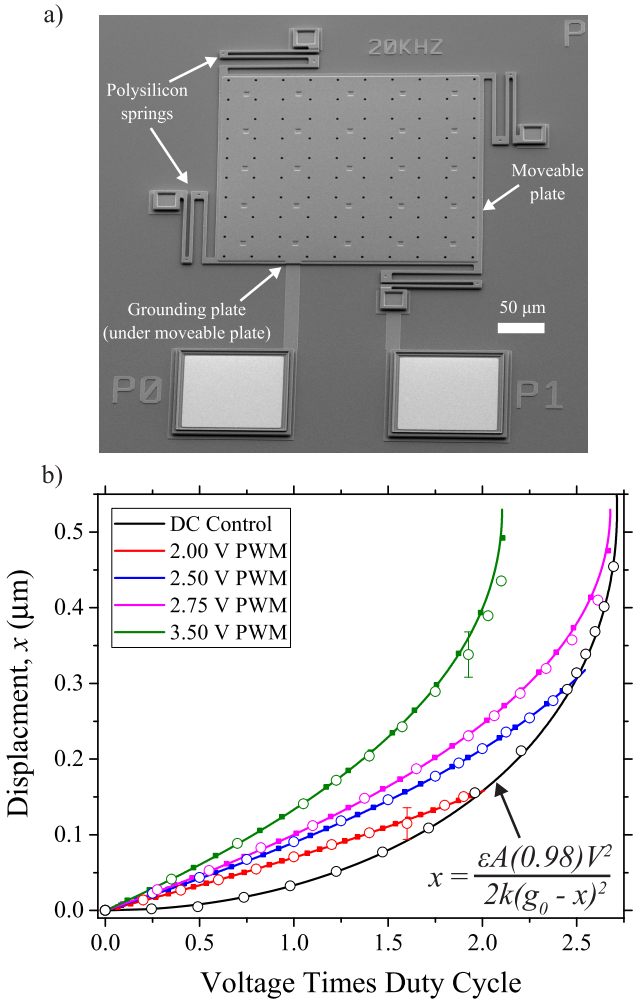

Fig. 2. **Parallel Plate:** a) SEM image of the parallel plate system used. b) Plot of the plate displacement versus voltage times duty cycle. The circles, squares and solid lines represent data, simulation and analytic results respectively. The black plot shows the response to voltage control. The 0.98 term in the equation is because we use a 98% duty cycle while varying the max voltage, V. The different colors, red, blue, purple, and green, represent PWM control at different maximum voltages, 2, 2.5, 2.75, and 3.5 V respectively. These results use a 300 kHz PWM frequency.

a 300 μm square movable plate suspended above a second 290 μm square grounding plate by four serpentine springs shown in Fig. 2a. All components are made of polysilicon. The two plates start 1.6 μm apart. The natural frequency of the device is 20 kHz. The plate is very stiff in comparison to the springs and the mass of the springs is small in comparison to the plate. This system is well represented as a lumped element model as shown in Fig. 1a.

Using a function generator, we produce a voltage difference between the two plates; causing the top plate to move closer to the grounding plate. A harmonic oscillator typically needs to be driven at a frequency greater than 10x the device natural frequency in order to sufficiently reduce the oscillatory response, therefore we use a 300 kHz PWM signal. Since the displacement of the device is normal to the substrate, we use a white light interferometer (Zygo NewView 6300) which has nanometer vertical resolution [38].

To study the effect of duty cycle and voltage we tested a number of different scenarios. The results are presented in Fig. 2b, each is represented by a different color, with black as the DC voltage control and the other colors (i.e. green, purple, blue, and red) as different PWM voltages. The x-axis of the plot is the PWM voltage times the duty cycle (0-1), which normalizes the data and makes it easier to compare the different data sets. The black curve holds a constant 98% duty cycle while increasing the voltage, whereas, the PWM drives hold a constant voltage while varying the duty cycle. The open circles are the experimental data points with error bars representing two standard deviations. Most of the error bars are smaller than the circles and are hidden. The solid lines represent the analytic solutions. For the PWM drives, we also include simulated results shown as the solid squares. The simulation uses an Euler method to numerically solve the steady state solution of equation (1) with a PWM signal input.

As previously mentioned, the black curve represents the displacement as a function of applied DC voltage. The analytic solution shown by the solid black line is included in the figure. We see the expected response with pull-in occurring at 1/3 of the pre-actuation gap (g_0) at approximately 2.75 V. The green, purple, blue and red curves are data using a PWM drive method, representing a PWM voltage of 3.5, 2.75, 2.50, and 2.00 V respectively. The analytic solution shown by these curves represent the solution to equations (7) and (9) with the measured plate geometry and voltages. These curves predict the data well, with only a slight deviation near pull-in. With the exception of the 3.5 V (green) scenario, the duty cycle is increased from 0% to 98% for each PWM drive. At 98% each curve matches up with its respective voltage on the DC voltage curve (black). The 3.5 V (green) case is an interesting data set because it uses a voltage that exceeds pull-in voltage of the device. For this reason, it does not intercept the DC voltage curve. Instead of increasing to 98% duty cycle, the 3.5 V PWM drive is only increased to 60% duty cycle, beyond which the plate pulls-in.

Comparing the the 2.00 V (red) response to the DC voltage control, we see that the displacement is linear as opposed to quadratic. However this only moves the plate 1/9 of the pre-actuation distance. We can increase the displacement by increasing the PWM voltage as shown in the green, purple, and blue curves. Initially these responses follow a linear trajectory, however as the plate approaches the pull-in distance they develop more curvature. By using a voltage greater than or equal to the pull-in voltage there is no loss in positional range compared to the DC control.

B. Comb-Drive Actuator

In Fig. 3a we show an optical microscope image of the second device we discuss in this paper. This device is an in-plane comb-drive actuator made with the same PolyMUMPs process as the parallel plate. The comb-drive consists of 31 interdigited polysilicon fingers, each 3.5 μm thick and with a 2.0 μm gap between each finger. It uses a polysilicon folded beam suspension for the spring force. The natural frequency of this device is 1 kHz, therefore we used a PWM frequency

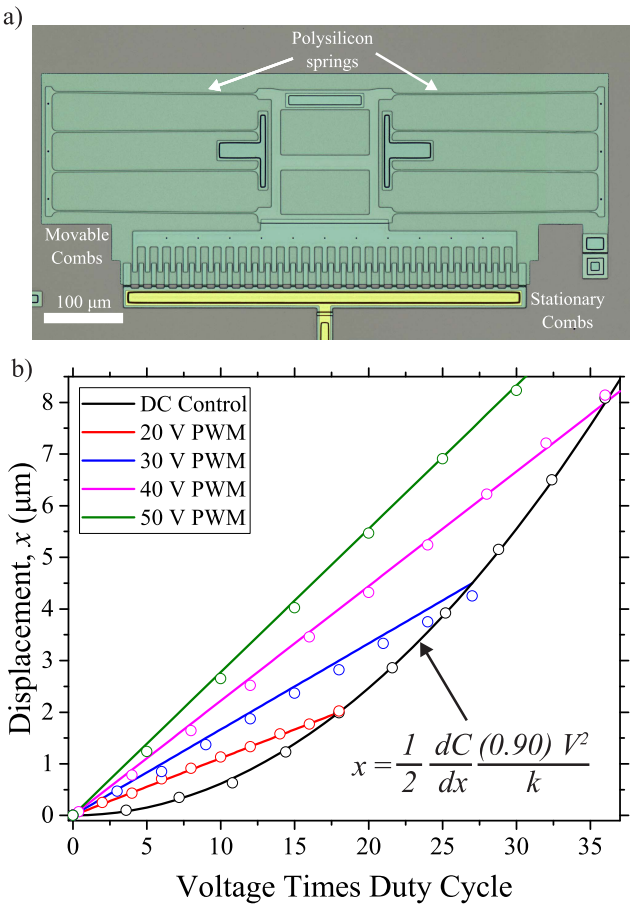

Fig. 3. **Comb-Drive:** a) Optical microscope image of the comb-drive system used. b) Plot of the comb displacement versus voltage times duty cycle. The circles and solid lines represent data and analytic results respectively. The black plot shows the response to voltage control. The 0.90 term in the equation is because we use a 90% duty cycle while varying the max voltage, V. The different colors, red, blue, purple, and green, represent PWM control at different maximum voltages, 20, 30, 40, and 50 V respectively. These results use a 50 kHz PWM frequency.

of 50 kHz. This system is well represented by our comb-drive model in Fig. 1b.

Unlike the parallel plate actuator, this device has a pull-in voltage close to 40 V. To generate the higher voltages, we use a high speed, HV amplifier (Trek 2100HF) to amplify the output of a function generator. Comb-drives move laterally in-plane, therefore we can use an optical microscope to image and measure the displacement of the movable fingers.

We use a similar approach to study the effect of duty cycle and voltage on the comb-drive as we do with the parallel plate. The results are shown in Fig. 3b. Again, each color represents a different driving scenario with black as the DC voltage control and the other colors (i.e. green, purple, blue and red) as different PWM voltages. The DC voltage curve holds a constant 90% duty cycle while increasing the voltage, whereas, the PWM drives hold a constant voltage while varying the duty cycle. The open circles are the experimental data points and the solid lines represent the analytic solutions.

The analytic solutions use equation (8) instead of equation (10) due to the aforementioned fringe field effects. We use an

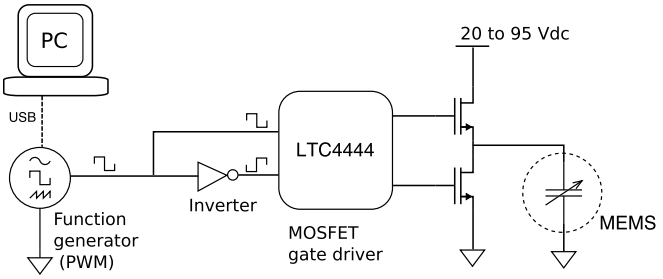

Fig. 4. **Low Cost Switching Circuit:** Simplified diagram of the N-channel MOSFET gate driver based circuit implemented to drive the DM using a high voltage PWM signal. We use a 92 V battery as the voltage source.

optical microscope to measure the comb-drive geometry and use these measurements in Comsol Multiphysics to simulate a value for dC/dx. This method accounts for both fringe field effects and the well known levitation effect [39]–[41], neither of which is captured by equation (10). It is worth noting that the analytic solutions shown in Fig. 3b use a single constant value for dC/dx. We also use Comsol simulate the spring constant of the comb-drive's folded beam suspension. The spring constant value is decreased 22% to best match the data. We attribute the difference largely to errors in the measurements of beam width and differences in material properties between our actual device and simulation.

The DC voltage control is represented by black, with the solid black line representing the analytic solution, which is included in the figure. We see the expected quadratic position response in Fig. 3b. Again we normalize the data by plotting the voltages times the duty cycle. The pull-in voltage and distance is less easily defined for the comb-drive compared to the parallel plate because it typically occurs due to either asymmetries in the device or small perturbations while actuating [36], both of which are difficult to predict. Nonetheless, we are able to experimentally determine that the pull-in voltage for the comb-drive is approximately 40 V. The green, purple, blue, and red represent a 50, 40, 30, and 20 V PWM signal respectively. The solid lines represent the solution to equations (7) and (10) with the measured geometry and voltage. As we see in Fig. 3b the theory predicts the linear response well. With the exception of the 50 V case (green), we increase the duty cycle from 0% to 90% for each PWM drive. At 90% each curve matches up with its respective voltage on the DC control curve. The 50 V scenario again is noteworthy as it uses a PWM voltage which exceeds the pull-in voltage of the device. Therefore it does not match up with a data point on the voltage control curve. Instead the 50 V case increases from 0% to 60% duty cycle. Increasing the duty cycle beyond 60% causes the comb-drive to pull-in.

Unlike the parallel plate actuator, the position response of the comb-drive with respect to duty cycle is completely linear throughout the full range of motion, regardless of position or driving voltage. We can see why by examining equation (10). The force on the comb-drive does not change with position. By switching a constant force on and off, the response is linear with respect to the duty cycle. Like the parallel plate, there is no loss of motion in the actuator when using a PWM voltage greater than or equal to the pull-in voltage.

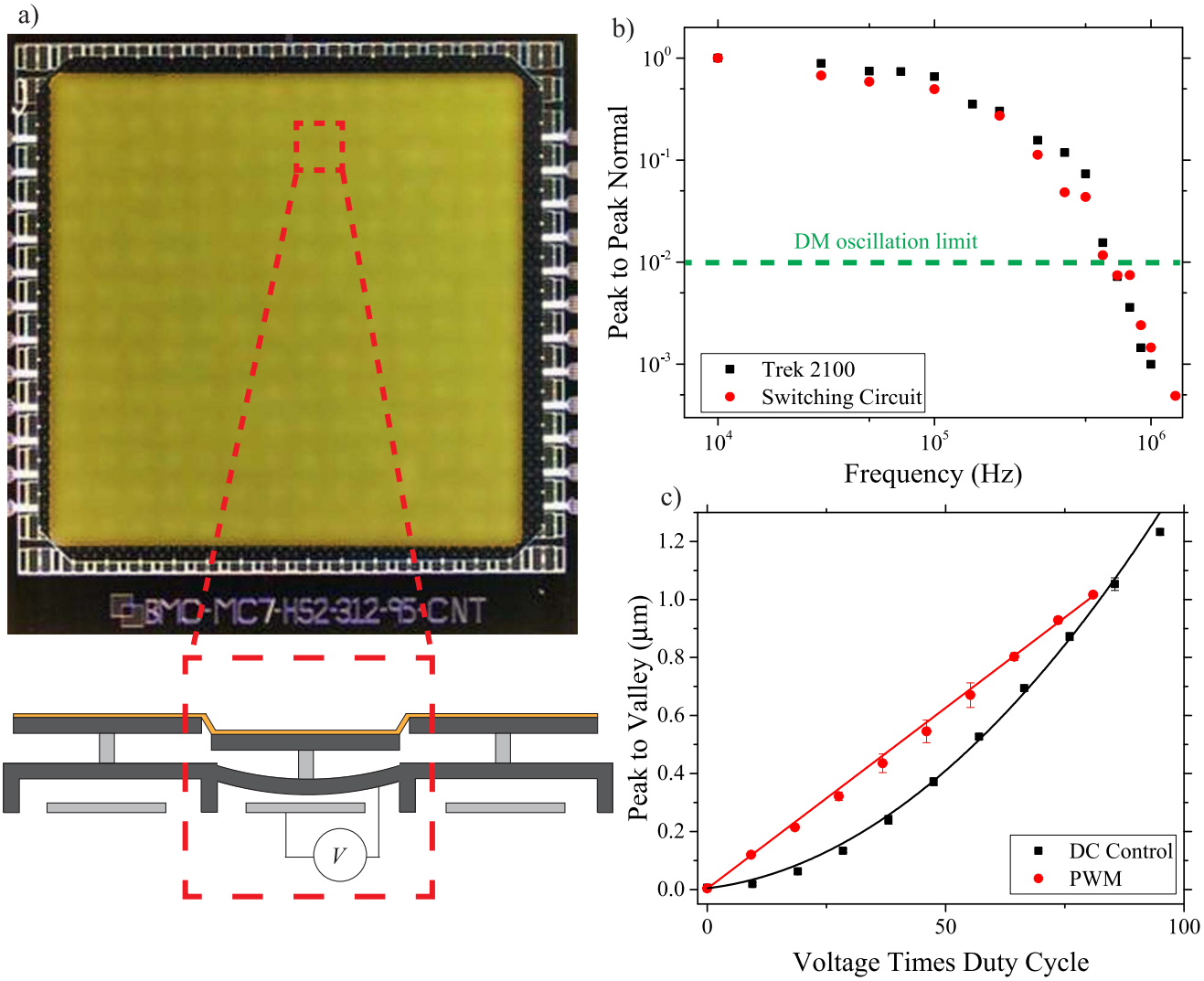

Fig. 5. **Deformable Mirror:** a) Optical image and graphical model of the DM parallel plate capacitor. The red square highlights a single parallel plate actuator. b) The normalized peak to peak frequency response of a single actuator in the DM array. We use a 50% duty cycle PWM between 0 and 92V. Black data shows the results using a high frequency HV amplifier and the red data shows the results from using a low cost switching circuit. The data is normalized to the 10 kHz response. The green dashed line represents the limit for acceptable oscillations for the DM. c) The steady state peak to valley displacement of the DM actuator versus voltage times duty cycle. The black data shows the DC voltage response and the red data shows the PWM control response. The red and black lines are linear and quadratic fits to the data respectively. The PWM drive switches between 0 and 92 V at a PWM frequency of 700 kHz.

C. Commercial DM

In Fig. 5a we show the third device, a commercial MEMS DM (BMC MultiDM) built by Boston Micromachines Corporation. The mirror consists of a continuous layer of gold spread over an array of 140 parallel plate type actuators. The vertical position of each actuator can be independently controlled. The DM is used widely in applications in astronomy and biomicroscopy [42]–[46]. The basic DM architecture has been reported previously [47], along with models and measurements of its electrostatic behavior [48]. The device used in this study features electrostatic actuators with dimensions and characteristics similar to those described in [49]. The device shown has a total of 140 actuators and we present data on the deflection of the mirror surface directly above one of those actuators. The DM operates at voltages greater than 100 V. The comb-drive setup uses an expensive amplifier to prove the concept and compare to the analytic solution, however we also want to show that PWM can be used as a low cost method. In that regard, we use two high voltage methods to drive the DM, (1) a low cost, high speed, high voltage switching circuit and (2) the same amplifier as the comb-drive setup for comparison. The switching circuit consists of a high voltage gate drive, a pair of transistors, a handful of other electrical components and a high voltage source (i.e. 92 V battery). A simplified schematic of the circuit is shown in Fig. 4. We use a function generator to vary the frequency and duty cycle of a PWM signal with a fixed amplitude of 5 V. The two LTC4444 inputs are supplied with the unaltered and inverted PWM signal and its two outputs drive the two N channel MOSFETs connected to the MEMS device. The LTC4444 can operate up to 100 V with rise and fall switching time in the order of 10 ns for a 1 nF capacitive load. The point is not to present this circuit as “the low cost solution” but instead to

provide an example of how PWM can be implemented cheaply to drive a high voltage electrostatic MEMS device. Although we use a computer and function generator to produce the PWM signal in this experiment, these could be replaced by a cheap microprocessor or a field programmable gate array.

We first test the frequency response of the DM using both the Trek 2100HF amplifier and our switching circuit to provide a 50% duty cycle PWM signal switching between 0 and 92 V. We use a Polytec vibrometer to measure the velocity of the piston mode actuation and integrate this to get a displacement. Testing the frequency response accomplishes two things: (1) it compares the switching circuit to the amplifier to ensure similar results and (2) provides a measurement of the oscillation amplitude. To operate properly the normalized oscillation amplitude needs to be less than 0.01 and we can experimentally determine the necessary frequency. Fig. 5b shows that the performance of the switching circuit and amplifier are comparable. This gives us confidence moving forward that we can use the switching circuit in place of the amplifier. Fig. 5b also shows that the oscillation of the DM drops below the amplitude limit at 700 kHz. We use this frequency to demonstrate the steady state response.

For the steady state response, we use the white light interferometer to measure the vertical displacement of the mirror. Fig. 5c shows a central result of this paper. The DC voltage control is shown in black with data points as solid black squares and the solid line is a quadratic fit to the data. Here we use a 100% duty cycle and increase the voltage to 95 V. The PWM data is shown in red circles and the red line is a linear fit. The PWM drive uses a 92 V signal and increases from 0% to 88% duty cycle. Fig. 5c shows that this curve intercepts the voltage control at the respective voltage. At this voltage, the response of the actuator is linear with respect to duty cycle. The pull-in voltage of this actuator is upwards of 200 V. The linear response using a 92 V PWM voltage correlates well with the results from the first device where we see a linear response at voltages lower than pull-in.

The results from these three devices summarize the advantages of the PWM drive method: (1) PWM can map out the entire response curve of the conventional analog approach, (2) the response can be a linear function of duty cycle, eliminating the standard non-linear response one finds with analog control and (3) by using a high voltage switch instead of a DAC and a linear HV amplifier, one can control the device with timing, not analog control. Although we use a HV amplifier to demonstrate the capability and limitations of the PWM with the comb-drive device, this could be replaced by a low cost switching circuit similar to the one shown in Fig. 4. The current electronics circuit to control the DM is a majority of the system price, with the components for each channel costing approximately \$10. Using quantities comparable to the commercial DM, we estimate the components for the circuit in Fig. 4 to cost approximately \$3.00/channel, $\sim$3 times less expensive. For the DM in this work, which has 140 channels, that is a \$980 cheaper. The main reason for this lower cost is because the circuit uses components that are manufactured at a larger quantity. A HV linear amplifier is a more specialized component than a HV transistor; this results in lower manufacturing volumes and higher prices. Such a cost reduction is significant and opens up the application space for the use of such DM systems. The main limitation to the PWM approach is that it excites the mechanical modes of the system. However, these oscillations can be reduced to an acceptable level by increasing the drive frequency as shown in Fig. 5b. With advancements in the electronics industry, PWM continues to get faster, cheaper, and easier to implement.

IV. Conclusion

In this paper we discussed the use of a PWM signal to control analog MEMS devices compared to the conventional method. We demonstrated that by applying a PWM signal to a MEMS device at frequencies well above the device natural frequency, one can achieve precise, analog control. This can be done with no loss in range compared to the conventional analog approach and allows system designers to replace expensive electronic components such as high precision DACs and HV linear amplifiers with a low cost switching circuit. In addition, research and development into transistors by the electronics industry continues to improve transistor speeds and this approach exploits these long term trends to create low cost control circuits. We have also demonstrated how it can linearize the positional response of devices where typically the position would depend quadratically on the applied, analog voltage.

Acknowledgment

The author Prof. T. G. Bifano acknowledges a financial interest in Boston Micromachines Corporation, which produced some of the hardware test devices that were studied in this work.

References

[1] J. Morrison, M. Imboden, T. D. C. Little, and D. J. Bishop, "Electrothermally actuated tip-tilt-piston micromirror with integrated varifocal capability," *Opt. Express*, vol. 23, no. 7, pp. 9555–9566, 2015.

[2] S. T. S. Holmström, U. Baran, and H. Urey, "MEMS laser scanners: A review," *J. Microelectromech. Syst.*, vol. 23, no. 2, pp. 259–275, 2014.

[3] D. M. Marom *et al.*, "Wavelength-selective 1 × K switches using free-space optics and MEMS micromirrors:Theory, design, and implementation," *J. Lightw. Technol.*, vol. 23, no. 4, pp. 1620–1630, Apr. 2005.

[4] M. J. Li *et al.*, "Microshutter array system for james webb space telescope," *Proc. SPIE*, vol. 6687, p. 668709, Sep. 2007. [Online]. Available: https://www.spiedigitallibrary.org/conference-proceedings-of-spie/6687/668709/Microshutter-array-system-for-James-Webb-Space-Telescope/10.1117/12.734152.full?SSO=1

[5] J. Collier, D. Wroblewski, and T. Bifano, "Development of a rapid-response flow-control system using MEMS microvalve arrays," *J. Microelectromech. Syst.*, vol. 13, no. 6, pp. 912–922, Dec. 2004.

[6] K. Entesari and G. M. Rebeiz, "A 12-18-GHz three-pole RF MEMS tunable filter," *IEEE Trans. Microw. Theory Techn.*, vol. 53, no. 8, pp. 2566–2571, Aug. 2005.

[7] K. Chen, X. Liu, A. Kovacs, W. J. Chappell, and D. Peroulis, "Antibiased electrostatic RF MEMS varactors and tunable filters," *IEEE Trans. Microw. Theory Techn.*, vol. 58, no. 12, pp. 3971–3981, Dec. 2010.

[8] X. Liu, K. Kim, and Y. Sun, "A MEMS stage for 3-axis nanopositioning," *J. Micromech. Microeng.*, vol. 17, no. 9, pp. 1796–1802, 2007.

[9] Q. Yao, J. Dong, and P. M. Ferreira, "Design, analysis, fabrication and testing of a parallel-kinematic micropositioning *XY* stage," *Int. J. Mach. Tools Manuf.*, vol. 47, no. 6, pp. 946–961, 2007.

[10] M. Maroufi, A. G. Fowler, and S. O. R. Moheimani, "MEMS for nanopositioning: Design and applications," *J. Microelectromech. Syst.*, vol. 26, no. 3, pp. 469–500, Jun. 2017.

[11] P. G. del Corro, M. Imboden, and D. J. Pérez, D. J. Bishop, and H. Pastoriza, "Single ended capacitive self-sensing system for comb drives driven *XY* nanopositioners," *Sens. Actuators A, Phys.*, vol. 271, pp. 409–417, Mar. 2018.

[12] M. Imboden *et al.*, "Atomic calligraphy: The direct writing of nanoscale structures using a microelectromechanical system," *Nano Lett.*, vol. 13, no. 7, pp. 3379–3384, 2013.
[13] J. D. Grade, H. Jerman, and T. W. Kenny, "Design of large deflection electrostatic actuators," *J. Microelectromech. Syst.*, vol. 12, no. 3, pp. 335–343, Jun. 2003.
[14] J. I. Seeger and B. E. Boser, "Charge control of parallel-plate, electrostatic actuators and the tip-in instability," *J. Microelectromech. Syst.*, vol. 12, no. 5, pp. 656–671, Oct. 2003.
[15] G. N. Nielson and G. Barbastathis, "Dynamic pull-in of parallel-plate and torsional electrostatic MEMS actuators," *J. Microelectromech. Syst.*, vol. 15, no. 4, pp. 811–821, Aug. 2006.
[16] R. Yeh, S. Hollar, and K. S. J. Pister, "Single mask, large force, and large displacement electrostatic linear inchworm motors," *J. Microelectromech. Syst.*, vol. 11, no. 4, pp. 330–336, Aug. 2002.
[17] S. Imai and T. Tsukioka, "A magnetic MEMS actuator using a permanent magnet and magnetic fluid enclosed in a cavity sandwiched by polymer diaphragms," *Precis. Eng.*, vol. 38, no. 3, pp. 548–554, 2014.
[18] D. Niarchos, "Magnetic MEMS: Key issues and some applications," *Sens. Actuators A, Phys.*, vol. 106, nos. 1–3, pp. 255–262, 2003.
[19] J. H. Comtois and V. M. Bright, "Applications for surface-micromachined polysilicon thermal actuators and arrays," *Sens. Actuators A, Phys.*, vol. 58, no. 1, pp. 19–25, 1997.
[20] Q.-A. Huang and N. K. S. Lee, "Analysis and design of polysilicon thermal flexure actuator," *J. Micromech. Microeng.*, vol. 9, no. 1, pp. 64–70, 1999. [Online]. Available: papers2://publication/uuid/6267D293-24DE-4C18-A4B2-365734E9D23A
[21] D. Yan, A. Khajepour, and R. Mansour, "Design and modeling of a MEMS bidirectional vertical thermal actuator," *J. Micromech. Microeng.*, vol. 14, no. 7, pp. 841–850, 2004.
[22] N. Ledermann *et al.*, "1 0 0-Textured, piezoelectric $Pb(Zr_x, Ti_{1-x})O_3$ thin films for MEMS: Integration, deposition and properties," *Sens. Actuators A, Phys.*, vol. 105, no. 2, pp. 162–170, 2003.
[23] P. F. van Kessel, L. J. Hornbeck, R. E. Meier, and M. R. Douglass, "A MEMS-based projection display," *Proc. IEEE*, vol. 86, no. 8, pp. 1687–1704, Aug. 1998.
[24] L. Svilainis, "LED brightness control for video display application," *Displays*, vol. 29, no. 5, pp. 506–511, 2008, doi: 10.1016/j.displa.2008.05.002.
[25] B. Bae *et al.*, "Feasibility test of an electromagnetically driven valve actuator for glaucoma treatment," *J. Microelectromech. Syst.*, vol. 11, no. 4, pp. 344–354, Aug. 2002.
[26] J. T. Butler, V. M. Bright, and W. D. Cowan, "Average power control and positioning of polysilicon thermal actuators," *Sens. Actuators A, Phys.*, vol. 72, no. 1, pp. 88–97, 1999.
[27] M. T. Bohr and I. A. Young, "CMOS scaling trends and beyond," *IEEE Micro*, vol. 37, no. 6, pp. 20–29, Nov./Dec. 2017.
[28] G. S. Tulevski *et al.*, "Toward high-performance digital logic technology with carbon nanotubes," *ACS Nano*, vol. 8, no. 9, pp. 8730–8745, 2014.
[29] T. N. Theis and P. M. Solomon, "In quest of the 'next switch': Prospects for greatly reduced power dissipation in a successor to the silicon field-effect transistor," *Proc. IEEE*, vol. 98, no. 12, pp. 2005–2014, Dec. 2010.
[30] P. Carbone, S. Kiaei, and F. Xu, *Design, Modeling and Testing of Data Converters*. Berlin, Germany: Springer-Verlag, 2014. [Online]. Available: http://www.springer.com/series/4748
[31] C. Pollock *et al.*, "Engineered PWM drives for achieving rapid step and settle times for MEMS actuation," *J. Microelectromech. Syst.*, vol. 27, no. 3, pp. 513–520, 2018.
[32] J.-F. Saheb, J.-F. Richard, M. Sawan, R. Meingan, and Y. Savaria, "System integration of high voltage electrostatic MEMS actuators," *Analog Integr. Circuits Signal Process.*, vol. 53, no. 1, pp. 27–34, 2007.
[33] S. Heinz *et al.*, "High-voltage amplifier design for MEMS based switching arrays in wavelength-division multiplexing networks," in *Proc. IEEE Int. Symp. Ind. Electron.*, Jun. 2007, pp. 1418–1423.
[34] J. Wu and L. R. Carley, "Electromechanical $\Delta\Sigma$ modulation with high-Q micromechanical accelerometers and pulse density modulated force feedback," *IEEE Trans. Circuits Syst. I, Reg. Papers*, vol. 53, no. 2, pp. 274–287, Feb. 2006.
[35] B. H. Tongue, *Principles of Vibration*, 2nd ed. New York, NY, USA: Oxford Univ. Press, 2002.
[36] M. I. Younis, *MEMS Linear and Nonlinear Statics and Dynamics*. New York, NY, USA: Springer, 2011.
[37] W.-M. Zhang, H. Yan, Z.-K. Peng, and G. Meng, "Electrostatic pull-in instability in MEMS/NEMs: A review," *Sens. Actuators A, Phys.*, vol. 214, pp. 187–218, Aug. 2014.
[38] *Newview 6300 Specifications*, Zygo, Berwyn, PA, USA, 2005.
[39] W. C. Tang, M. G. Lim, and R. T. Howe, "Electrostatic comb drive levitation and control method," *J. Microelectromech. Syst.*, vol. 1, no. 4, pp. 170–178, Dec. 1992.
[40] M. Imboden, J. Morrison, E. Lowell, H. Han, and D. J. Bishop, "Controlling levitation and enhancing displacement in electrostatic comb drives of MEMS actuators," *J. Microelectromech. Syst.*, vol. 23, no. 5, pp. 1063–1072, Oct. 2014.
[41] P. G. del Corro, M. Imboden, D. J. Bishop, and H. Pastoriza, "Comb drive designs with minimized levitation," *J. Microelectromech. Syst.*, vol. 25, no. 6, pp. 1025–1032, 2016.
[42] T. Bifano, "Adaptive imaging MEMS deformable mirrors," *Nature Photon.*, vol. 5, no. 1, pp. 21–23, 2011, doi: 10.1038/nphoton.2010.297.
[43] W. J. Shain, N. A. Vickers, B. B. Goldberg, T. Bifano, and J. Mertz, "Extended depth-of-field microscopy with a high-speed deformable mirror," *Opt. Lett.*, vol. 42, no. 5, pp. 995–998, 2017. [Online]. Available: https://www.osapublishing.org/abstract.cfm?URI=ol-42-5-995
[44] D. Sinefeld, H. P. Paudel, D. G. Ouzounov, T. G. Bifano, and C. Xu, "Adaptive optics in multiphoton microscopy: Comparison of two, three and four photon fluorescence," *Opt. Express*, vol. 23, no. 24, pp. 31472–31483, 2015. [Online]. Available: https://www.osapublishing.org/abstract.cfm?URI=oe-23-24-31472
[45] J. Li, T. G. Bifano, and J. Mertz, "Widefield fluorescence microscopy with sensor-based conjugate adaptive optics using oblique back illumination," *Proc. SPIE*, vol. 21, no. 12, p. 121504, 2016.
[46] B. Macintosh *et al.*, "The gemini planet imager: First light," *Proc. Nat. Acad. Sci. USA*, vol. 111, no. 35, pp. 2661–2666, 2014.
[47] T. G. Bifano, J. Perreault, R. K. Mali, and M. N. Horenstein, "Microelectromechanical deformable mirrors," *IEEE J. Sel. Topics Quantum Electron.*, vol. 5, no. 1, pp. 83–89, Jan./Feb. 1999.
[48] M. N. Horenstein, T. G. Bifano, R. K. Mali, and N. Vandelli, "Electrostatic effects in micromachined actuators for adaptive optics," *J. Electrostatics*, vol. 42, pp. 69–81, Oct. 1997.
[49] S. A. Cornelissen, P. A. Bierden, T. G. Bifano, and C. L. V. Lam, "4096-element continuous face-sheet MEMS deformable mirror for high-contrast imaging," *Proc. SPIE*, vol. 8, no. 3, p. 031308, 2009.

Corey Pollock received the B.S. degree in mechanical engineering from the University of Washington in 2010, and the M.S. degree in mechanical engineering from Boston University in 2017, where he is currently pursuing the Ph.D. degree in mechanical engineering, as a member of Dr. David Bishop's Group. His research involves MEMS technology, specifically studying micro mirrors and smart lighting applications.

Lawrence K. Barrett received the B.S. degree in applied physics, and the M.S. degree in physics from Brigham Young University in 2014 and 2015, respectively. He is currently pursuing the Ph.D. degree in materials science and engineering with Boston University. His research interests include MEMS design and control, nanomanufacturing, carbon nanotubes, graphene, and advanced chemical vapor deposition techniques.

Pablo G. del Corro received the B.S. degree in electronic engineering from the Universidad Nacional de Santiago del Estero, Argentina, in 2012, and the Ph.D. diploma degree in engineering sciences from Instituto Balseiro, Argentina, in 2017. His Ph.D. thesis was focused on the design and characterization of MEMS devices and control circuit implementation for a MEMS-based 3D printing system. He held post-doctoral positions at Bordeaux University, France, in 2018. His research focuses on using MEMS for sensing and energy harvesting applications.

Alexander Stange received the B.Sc. degree in physics from McGill University in 2012, and the M.Sc. in Engineering degree in nanotechnology from the University of Pennsylvania in 2016. He is currently pursuing the Ph.D. degree with the Material Science Division, Boston University (BU). At BU, he is currently researching the Casimir Effect using MEMS accelerometers and superconducting cavities. He is a member of the American Physical Society and the Materials Research Society.

Thomas G. Bifano received the B.S. and M.S. degrees in mechanical engineering and materials science from Duke University, Durham, NC, USA, and the Ph.D. degree in mechanical engineering from North Carolina State University, Raleigh, NC, USA. He is currently a Professor of mechanical engineering with Boston University, Boston, MA, USA, with joint appointment as a Professor with the Department of Biomedical Engineering and the Division of Materials Science and Engineering. His research focuses on development of microelectromechanical systems for optical and biomedical applications. He joined Boston University in 1988. He directs the Boston University Photonics Center, and is also the Co-Founder and the Chief Technology Officer of Boston Micromachines Corporation.

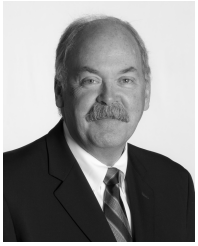

David J. Bishop received the B.S. degree in physics from Syracuse University, and the M.S. and Ph.D. degrees in physics from Cornell University. He was the Interim Associate Dean for Research and Graduate Programs at the College of Engineering, Boston University (BU). Before joining BU in 2011, he was the Chief Technology Officer, and also the Chief Operating Officer of LGS. Prior to joining LGS, he was the President of the Government Research & Security Solutions for Bell Labs, Lucent Technologies. He is currently the Director of the CELL-MET NSF Engineering Research Center, and the Head of the Division of Materials Science and Engineering, Boston University. He is also a Professor of physics, Professor of electrical and computer engineering, Professor of materials science and engineering, and a Professor of mechanical engineering. He is a Bell Labs Fellow. In his previous positions with Lucent, he served as the Nanotechnology Research VP for Bell Labs, Lucent Technologies, the President of the New Jersey Nanotechnology Consortium, and the Physical Sciences Research VP.